

## ***In vitro* Biomineralization Ability of Magnesium-Doped Coral Hydroxyapatite Coating Prepared by Pulsed Laser Deposition**

Xiaoxue Tan<sup>1</sup>, Peng Xue<sup>2</sup>, Hao Chen<sup>2</sup>, Xin Liu<sup>2</sup>, M.A. Yarmolenko<sup>1,3</sup>,  
Shangzhe Jiang<sup>4</sup>, Xiaohong Jiang<sup>1\*</sup>

<sup>1</sup>International Chinese-Belorussian Scientific Laboratory on Vacuum-Plasma Technology, Nanjing University of Science and Technology, 200, Xiaolingwei Street, Nanjing 210094, China

<sup>2</sup>The Affiliated Hospital of Nanjing University of Chinese Medicine, Department of Orthopedics, Nanjing 210029, China

<sup>3</sup>Francisk Skorina Gomel State University, 104, Sovetskaya street, Gomel 246019, Belarus

<sup>4</sup>British School of Nanjing, 16 Han Fu Lu, Jiangning, Nanjing 211106, China

### **Article info**

Received:  
15 March 2024

Received in revised form:  
28 April 2024

Accepted:  
11 June 2024

### **Keywords:**

Pulsed laser deposition  
Coral hydroxyapatite  
Magnesium  
Pore structure  
Mineralization *in vitro*

### **Abstract**

Coral hydroxyapatite (CHA) is a calcium phosphate that has a similar inorganic composition to human bone and the porous structure of coral stone. Due to its interconnected network like pore structure, it can serve as a framework for bone conduction. In this study, CHA films and Mg-CHA films were deposited on titanium and silicon substrates by Pulsed laser deposition, and then the films were heat treated respectively. Studies on the adhesion of the coating showed that the heat-treated Mg-CHA film adhered better to the titanium substrate. The experimental study on biomineralization *in vitro* showed that a small amount of porous structure appeared in the heat-treated Mg-CHA after immersion in SBF for three days, and the porous structure was visible after immersion for seven days. After 14 days, a new apatite layer formed on the surface. This suggested that magnesium undergoes chemical corrosion in SBF, leading to rapid ion exchange, which results in the formation of porous structures and promotes the development of an apatite-like layer. In summary, the heat-treated Mg-CHA films had superior biomineralization properties.

## **1. Introduction**

Bone defects resulting from trauma, inflammation, and tumors are common and complex issues in orthopedic clinical treatment [1]. Self-healing has limitations when it comes to the repair of larger bone defects, which poses a challenge in achieving satisfactory bone regeneration in such cases [2, 3]. Surgical treatment is commonly employed for the reconstruction of bone defects, including regenerative methods involving membrane techniques and implantation of bone graft substitutes [4]. Titanium-based implants are widely used in orthopedics for bone reconstruction. Titanium is known for

its high corrosion resistance and biocompatibility. However, a major drawback of titanium-based implants is their low osteointegration ability. One technological approach to enhance the osteointegration capability of metallic implants is the application of coatings on their surface that stimulate bone tissue growth [5]. Calcium phosphates exhibit excellent biocompatibility, meaning they are generally not rejected by the human body. This is because calcium phosphates naturally exist in both dissolved and solid forms within the body. Calcium phosphates are used as bone substitutes in orthopedics for treating bone defects [6].

Coral hydroxyapatite (CHA) has been proposed as the target material for deposition. It is derived from the skeleton of marine coral and has a chemical composition similar to human bone tissue [7, 8].

\*Corresponding author.

E-mail address: [jiangxh24@njjust.edu.cn](mailto:jiangxh24@njjust.edu.cn)

The presence of trace elements, such as magnesium and strontium, in coral hydroxyapatite exerts a stimulating effect on bone growth. These trace elements play a significant role in the absorbability and calcification process of CHA [9]. Compared to common hydroxyapatite, it has lower mechanical stability, specific surface area, wear resistance, and fracture toughness [10], but coral hydroxyapatite has an effectively homogeneous density and three-dimensional pore structure, while maintaining better support capacity and trabecular structure. This means that coral hydroxyapatite can not only be used as a bone defect repair material but can also function as an additional drug-releasing agent during the treatment process [11]. Overall, coral hydroxyapatite has potential as an artificial bone material in the field of bone defect repair, providing a viable option for bone reconstruction [12, 13].

In general, coatings deposited using vacuum methods do not possess the developed structure required for rapid nucleation and growth of bone tissue. To achieve a porous structure, the addition of magnesium to the target composition has been proposed. On one hand, magnesium is the fourth most abundant element naturally present in human bones and one of the essential ions in the body [14, 15]. Magnesium possesses good biocompatibility and osteogenic activity. It also promotes the adhesion of osteoblasts and the growth and formation of the bone matrix during the development of bone tissue [16, 17]. When the body is deficient in magnesium, it can lead to bone damage, making osteoblasts and osteoclasts less active, which increases the risk of developing osteoporosis [18, 19]. According to relevant research reports, magnesium is usually one of the doping reagents for calcium phosphate biomaterials [20, 21]. The addition of magnesium ions to bone implant materials can effectively promote the formation of new bone and significantly influence the crystallization and biodegradation of mineral substances [22, 23]. According to reports, magnesium-containing calcium phosphate materials are effective components for enhancing the biocompatibility of hydroxyapatite (HA) coatings. On the other hand, the rapid corrosion of magnesium in a physiological environment can lead to the formation of a porous structure in the coating, thereby enhancing the effectiveness of the coating in bone defect restoration [24, 25].

Currently, coatings based on hydroxyapatite (HA) are widely used for this purpose. There are numerous technological methods available for applying HA coatings, with the plasma spray method being the

most popular and in demand. This method allows for the deposition of thick coatings. However, a drawback of this method is the high-temperature exposure during the coating application on the implant surface and the high level of internal stresses in the coating. The temperature exposure can lead to changes in the mechanical properties of the implant, which is not desirable [26, 27]. High internal stresses can cause cracking and delamination of the coating from the implant when exposed to liquid biological environments. There is another approach to implant modification where it is not necessary to apply thick layers to initiate osseointegration. According to this approach, the coating should promote nucleation and growth of bone tissue in the biological environment. This principle is the basis for the use of bioactive glasses, where the key requirement is the presence of a developed surface [28, 29]. In this study, the pulsed laser deposition (PLD) method was proposed for coating deposition. The main advantage of this method is the absence of temperature impact on the implant during the deposition process. Films obtained using PLD exhibit excellent mechanical properties such as adhesion and hardness.

This study is the first to use natural coral bone, a novel approach highlights in this paper, combining it with magnesium powder to prepare Mg-CHA coatings by Pulsed Laser Deposition (PLD). The morphology, structure and biological properties of the films are determined and the effectiveness of these coatings in promoting bone tissue growth is evaluated.

## 2. Materials and methods

### 2.1 Material

Magnesium powder (Mg) with a particle size of 75–150  $\mu\text{m}$  was purchased from Sinopharm Chemical Reagent Co., Ltd (Shanghai, China). Coral Hydroxyapatite [ $\text{Ca}_{10}(\text{PO}_4)_6(\text{OH})_2$ , CHA] with a particle size of 0.25–1.0 mm was purchased from the Tooth-ease online medical device franchise store (Sichuan, China). Silicon chip was purchased from Suzhou Jing-si Electronic Technology Co., Ltd (Suzhou, China). Titanium foil was purchased from Wuxi Thousand Hammer Metal Products Co., Ltd. (Jiangsu, China). Modified-simulated body fluid was purchased from Phygene Biotechnology Co., Ltd (Fujian, China).

### 2.2 Preparation of the target

Pure CHA target disks were prepared by weighing coral hydroxyapatite and subjected to 10 MPa uniaxial pressing without using any calcination or

sintering processes; Weighing coral hydroxyapatite and magnesium powder (weight ratio = 1:1), the raw materials were poured into a mortar and ground until fully mixed, and then pressed to form a multi-component Mg-CHA target disk. Using pulsed laser deposition (PLD), a plasma plume was formed by laser ablation of the target, and the materials were finally deposited on titanium wafer substrates and silicon wafer substrates to form CHA coatings as well as Mg-CHA coatings.

### 2.3 Pulsed laser deposition

Two different substrates for titanium and silicon wafers were cut into 20 x 20 mm as substrates and cleaned in an ultrasonic cleaner with ultrapure water and anhydrous ethanol for 15 min and repeated 3 times, respectively. After washing, the substrate was dried in a vacuum oven at 80 °C for 4 hours. A Nd: YAG solid-state laser with a laser wavelength of 1064 nm, pulse duration, and repetition frequency of 18 ns and 10 Hz, respectively, was selected for coating preparation. After the targets and substrates were fixed, the chamber was evacuated and the pressure was maintained at  $\sim 6 \times 10^{-4}$  Pa. During the deposition process, the pressure was controlled at  $\sim 2 \times 10^{-3}$  Pa, and the target was rotated at 25 r/min to avoid the target being pierced by the laser, during the application process, the thickness of the coating was directly monitored using a quartz crystal microbalance (QCM), and the thickness is approximately 150 nm. By this method, CHA films and Mg-CHA films were deposited on the substrates of silicon and titanium wafers. In addition, part of the films were placed in a tubular furnace for heat treatment and protected by argon. The temperature was raised from room temperature at a heating rate of 5 °C/min and kept for 3 h after reaching 500 °C, and then followed by natural cooling to room temperature.

### 2.4 Material characterization

#### 2.4.1 Physicochemical characterization

The surface morphology of the film was analyzed using scanning electron microscopy (SEM; FEI Quanta 250FEG) equipped with energy-dispersive X-ray spectroscopy (EDAX, USA). The crystalline structure of the deposited film was characterized by X-ray diffraction (XRD, Bruker D8 ADVANCE). The elemental composition and chemical bonding of the surface film were obtained by X-ray photoelectron spectroscopy (XPS, PHI Quantera II) with Al K $\alpha$  mono-chrome X-rays ( $h\nu = 1486.6$  eV) source. The 3D topography

and square roughness ( $R_q$ ) of the film were obtained by atomic force microscopy (AFM, Bruker Dimension Icon). The adhesion of the film was measured by the scratch meter (Lanzhou Zhongke Kaihua Technology Development Company WS-2005). The scratch method was used to evaluate the bonding strength between the film and the substrate, while the toughness of the film was qualitatively rated using crack propagation resistances (CPRs). CPRs are calculated by the formula  $CPRs = Lc_1 \times (Lc_2 - Lc_1)$ . Among them,  $Lc$  is the load intensity (membrane substrate bonding force) when the film and substrate just detach,  $Lc_2$  is the maximum load when the film detaches from the substrate, and  $Lc_1$  is the initial load when the film first cracks. The pressure of the indenter gradually increases from 0 to 20 N, and a long strip-like scratch appears, from thin to wide, with a scratch length of 4mm, in line with the change in load.

#### 2.4.2 In vitro analysis in SBF

The films were immersed in SBF to evaluate the biomineralization behavior of the samples. The films were punched into 0.5 mm diameter discs with a hole puncher and soaked in SBF at 37 °C for 3, 7, 9, and 14 days, after which the samples were removed and the film surfaces were rinsed with ultrapure water and then placed in a vacuum drying oven at 80 °C for 24 hours. Concentration detection of Ca<sup>2+</sup> and Mg<sup>2+</sup> in SBF before and after immersion was performed using inductively coupled plasma mass spectrometry (ICP-MS, ThermoFisher I CAPQ). The surface morphology and elemental composition of the samples were analyzed by SEM, EDS, XPS, and XRD.

## 3. Results and discussion

### 3.1 Morphology and structure of coatings

Figure 1 shows the SEM and AFM morphology of CHA (a) and Mg-CHA (c) films as well as heat-treated CHA (b) and heat-treated Mg-CHA (d) films. From the SEM image, it can be seen that the surface morphology of the films before and after heat treatment did not show a significant difference. The scratch lines in the image are caused by the titanium substrate, rather than the morphology of the deposited film [30]. The  $R_q$  values of CHA film, heat-treated CHA film, Mg-CHA film, and heat-treated Mg-CHA film are 1.46 nm, 12.4 nm, 42.4 nm, and 20.0 nm, respectively. The significant increase in  $R_q$  value after magnesium doping may be due to the presence of fine grains of magnesium on the surface of the film.

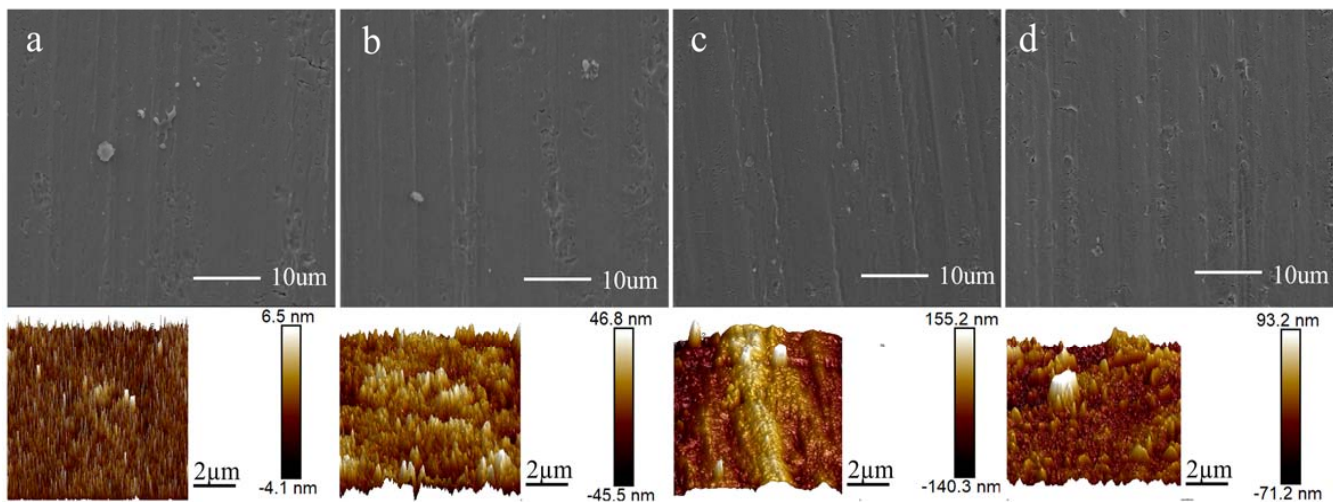


**Fig. 1.** SEM and AFM morphology of CHA and Mg-CHA films before and after heat treatment: (a) CHA film; (b) heat-treated CHA film; (c) Mg-CHA film; (d) heat-treated Mg-CHA film.

Heat treatment affects the grain size, which in turn decreases the Rq value of heat-treated Mg-CHA.

Figure 2a shows the XRD pattern of the CHA powder, which is consistent with the standard card of hydroxyapatite (HA) (JCDs# 09-0432). Figures 2b and 2c show that the characteristic diffraction peaks at 16.86°, 25.88°, 34.08°, and 35.49° of the CHA films before and after heat treatment correspond to HA (JCDs# 09-0432). The diffraction peaks at 40.10°, and 62.71° correspond to Ti (JCDs# 65-6231). This can indicate that the CHA films before and after heat treatment did not affect the peak positions as well as the crystalline shape changes. The CHA films can

cover the titanium sheet substrate to the extent that the peaks of the substrate are weak. Figures 2d and 2e show that a broad diffraction peak formed before 15°~35° corresponds to amorphous calcium phosphate (ACP). The diffraction peaks at 38.18°, 40.10°, 52.94°, and 62.71° correspond to the characteristic diffraction peaks of Ti (JCDs# 65-6231). As can be seen from the figure, the diffraction peaks of the other phases are significantly weakened because the diffraction peaks of the Ti substrate are too strong.

Figure 3 shows the XPS high-resolution spectrum of CHA (a) and Mg-CHA (c) films as well as heat-treated CHA (b) and heat-treated Mg-CHA (d)

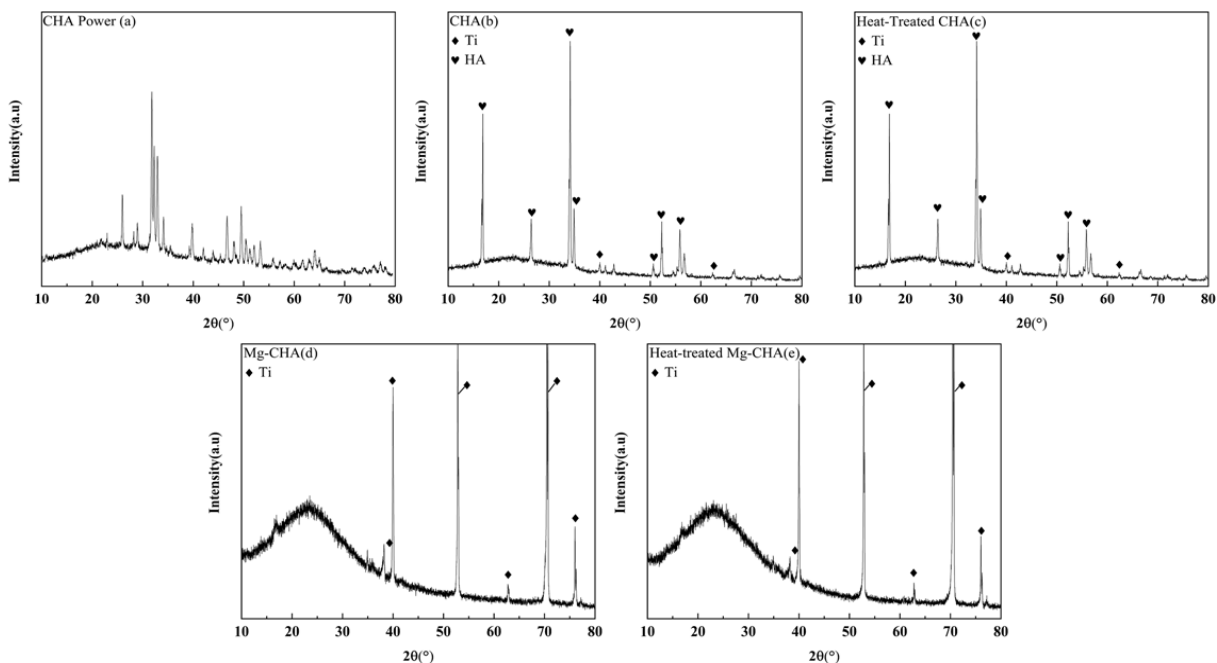


**Fig. 2.** XRD patterns of CHA and Mg-CHA films before and after heat treatment: (a) CHA power; (b) CHA film; (c) heat-treated CHA film; (d) Mg-CHA film; (e) heat-treated Mg-CHA film.

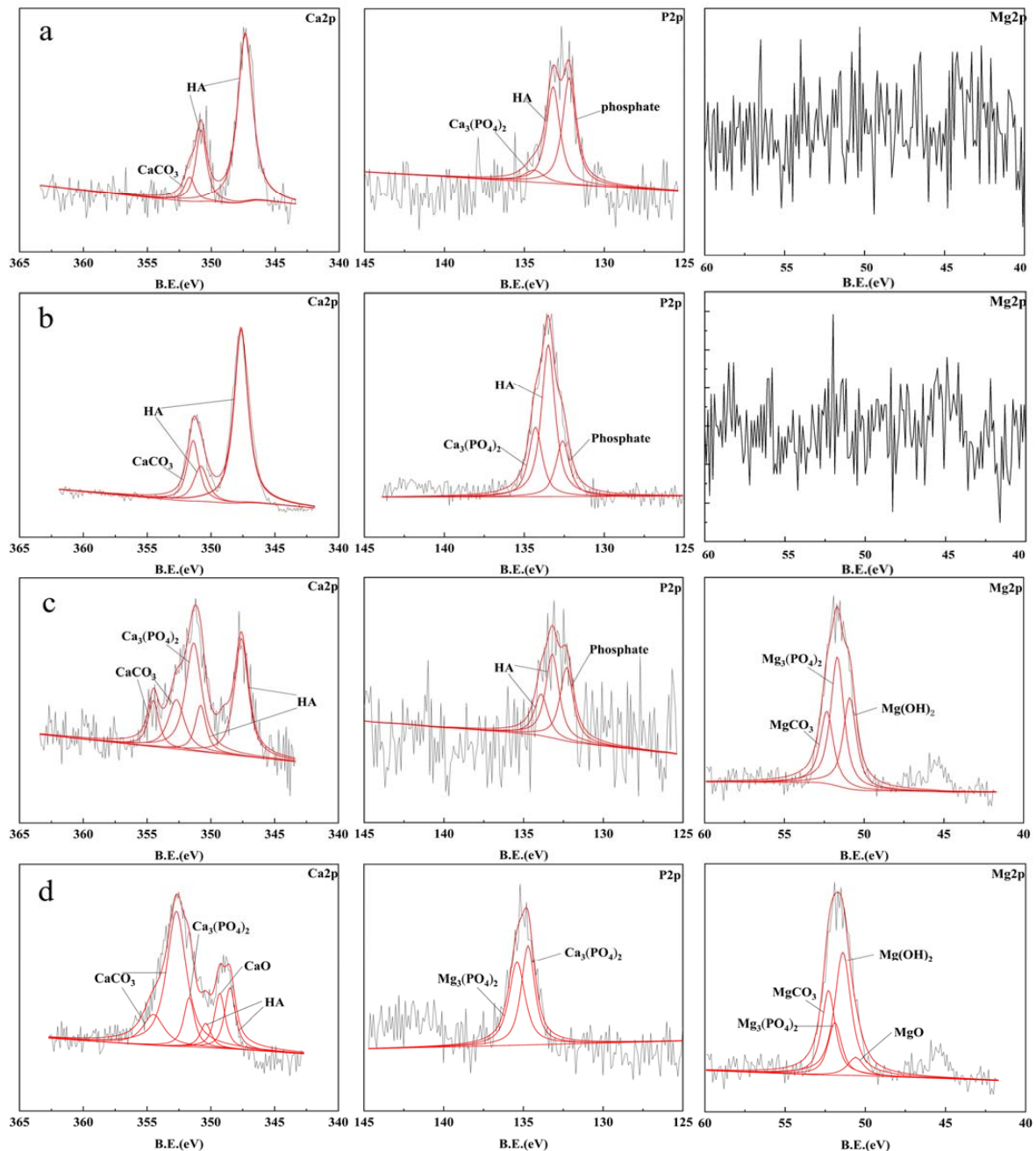


**Fig. 3.** XPS high-resolution mapping of Ca2p, P2p, and Mg2p in CHA and Mg-CHA films before and after heat treatment: (a) CHA film; (b) heat-treated CHA film; (c) Mg-CHA film; (d) heat-treated Mg-CHA film.

films. The Ca2p of the CHA film before and after heat treatment was simulated to form three characteristic peaks, namely 351 eV corresponding to Ca2p in  $\text{CaCO}_3$ , 350 eV, and 347 eV corresponding to Ca2p in HA [ $\text{Ca}_3(\text{PO}_4)_5\text{OH}$ ]. The Ca2p of Mg-CHA film before and after heat treatment corresponds to  $\text{CaCO}_3$ , 351 eV corresponding to  $\text{Ca}_3(\text{PO}_4)_2$  at 354 eV and 352 eV, where the heat-treated Mg-CHA films shows Ca2p of CaO at 349 eV.

In addition, the P2p of the sample is fitted for analysis. At 134 eV,  $(\text{PO}_4)^{3-}$  corresponds to  $\text{Ca}_3(\text{PO}_4)_2$ , the binding energy at 133 eV corresponds to  $(\text{PO}_4)^{3-}$  in HA, while at 132 eV, it belongs to other phos-

phates. The Mg-CHA after heat treatment is mainly synthesized into two peaks, namely  $\text{Mg}_3(\text{PO}_4)_2$  at 135 eV and  $(\text{PO}_4)^{3-}$  corresponding to  $\text{Ca}_3(\text{PO}_4)_2$  at 134 eV.

The high-resolution spectrum of Mg2p is fitted and analyzed, corresponding to  $\text{Mg}_2\text{CO}_3$  at 52.3 eV,  $\text{Mg}(\text{OH})_2$  at 51.3 eV, and  $\text{Mg}_3(\text{PO}_4)_2$  at 51.6 eV. For the Mg2p peak, it can be inferred that the peak at higher BE is related to oxygen such as  $\text{MgCO}_3$  or magnesium peroxide, where Mg exists in the form of  $(^{2+})$  [31]. Due to the heat treatment of the Mg-CHA film, the peak value related to MgO shifts to a lower BE (50.2~50.0 eV), so it corresponds to MgO at 50.5 eV [32].

The chemical composition of the deposited CHA coatings corresponds to the chemical composition of the original compound. Thermal treatment does not have a noticeable impact on the structure of the deposited coating. Thermal treatment promotes the oxidation of magnesium, resulting in the formation of MgO.

### 3.2 Adhesion of coatings

Figure 4 shows the scratch patterns of four thin film samples, a, b, c, and d. Changes in scratch morphology during indenter movement: i) Shallow indentations begin to appear and the film begins to deform; ii) Minor cracks are found, the width of the indentation gradually increases, and a small amount of groove marks appeared; iii) The crack continues to expand, and the fracture deformation texture on both sides of the groove is significantly deepened, with fish scale-like peeling marks appearing; iiiii) The load gradually increases to the maximum load, and large-scale film peeling occurs, resulting in complete failure of the film.

Compared with Lc in Table 1, it can be found that the overall bonding strength of the heat-treated films (c, d) is greater than that of the untreated films (a, b). This is because the heat treatment is conducive to the secondary growth of film grains, allowing the film to completely cover the substrate surface, thereby improving the strength of the bonding force.

Figure 5 shows the XPS etching analysis of four kinds of films. The results show that a stable chemical bond  $\text{CaTiO}_3$  is formed between the heat-treated film and the titanium substrate, and  $\text{CaTiO}_3$  is found when heat-treated Mg-CHA is etched down a third time, which improves the overall bonding

strength of the film, so the overall film substrate bonding force is also better. By comparing CPRs, it was found that Mg-CHA has better toughness than CHA. Overall, the mechanical properties reflected by the scratch method of Mg-CHA film are better than those of CHA film. Doping Mg can significantly improve the overall mechanical properties of the film, and the bonding strength after heat treatment is improved. This result is consistent with the scratch method.

**Table 1.** Loads of four film samples  $\text{Lc}_1$ , Lc,  $\text{Lc}_2$  with CPRs (a) CHA film, (b) Mg-CHA film, (c) heat-treated CHA film, (d) heat-treated Mg-CHA film

Loads of four film samples $\text{Lc}_1$ , Lc, $\text{Lc}_2$ with CPRs				
Sample number	$\text{Lc}_1/\text{N}$	Lc/N	$\text{Lc}_2/\text{N}$	CPRs
a	1	12.4	17.1	16.1
b	1.1	12.9	17.3	17.8
c	1	13.1	16.7	15.7
d	1.1	13.27	16.4	16.8

### 3.3 In vitro biomineralization of coatings

Figure 6 shows the SEM morphology of Mg-CHA thin films soaked in SBF for 0, 3, 7, and 14 days after heat treatment. In Fig. 6a, the surface is pitted and the basal scar line is more pronounced. After 3 days of immersion, a small number of pore-like structures can be seen emerging in Fig. 6b, and coral bone-like structures can be seen. The pores are approximately 300–500 nm in size and are distributed over a relatively small area. Figure 6 c shows the image after soaking for 7 days, completely presenting a pore-like structure, and the contour of the

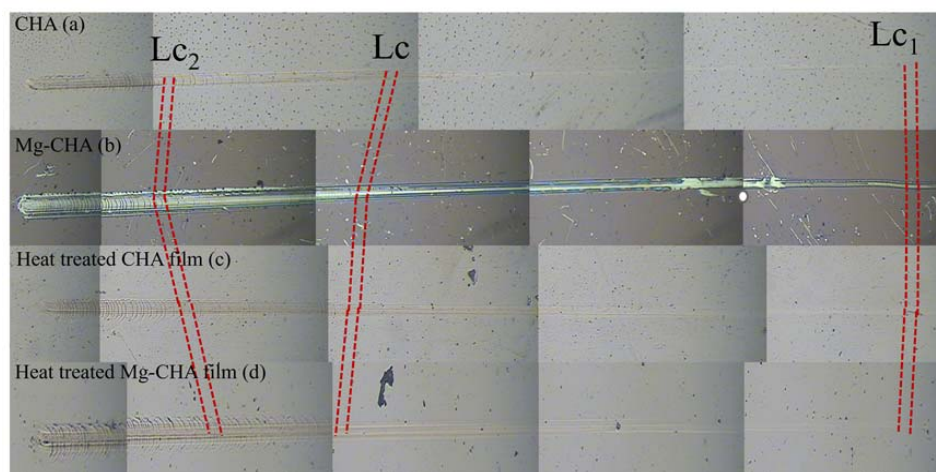


**Fig. 4.** Scratch diagrams of four film samples. (a) CHA film, (b) Mg-CHA film, (c) heat-treated CHA film, (d) heat-treated Mg-CHA film.

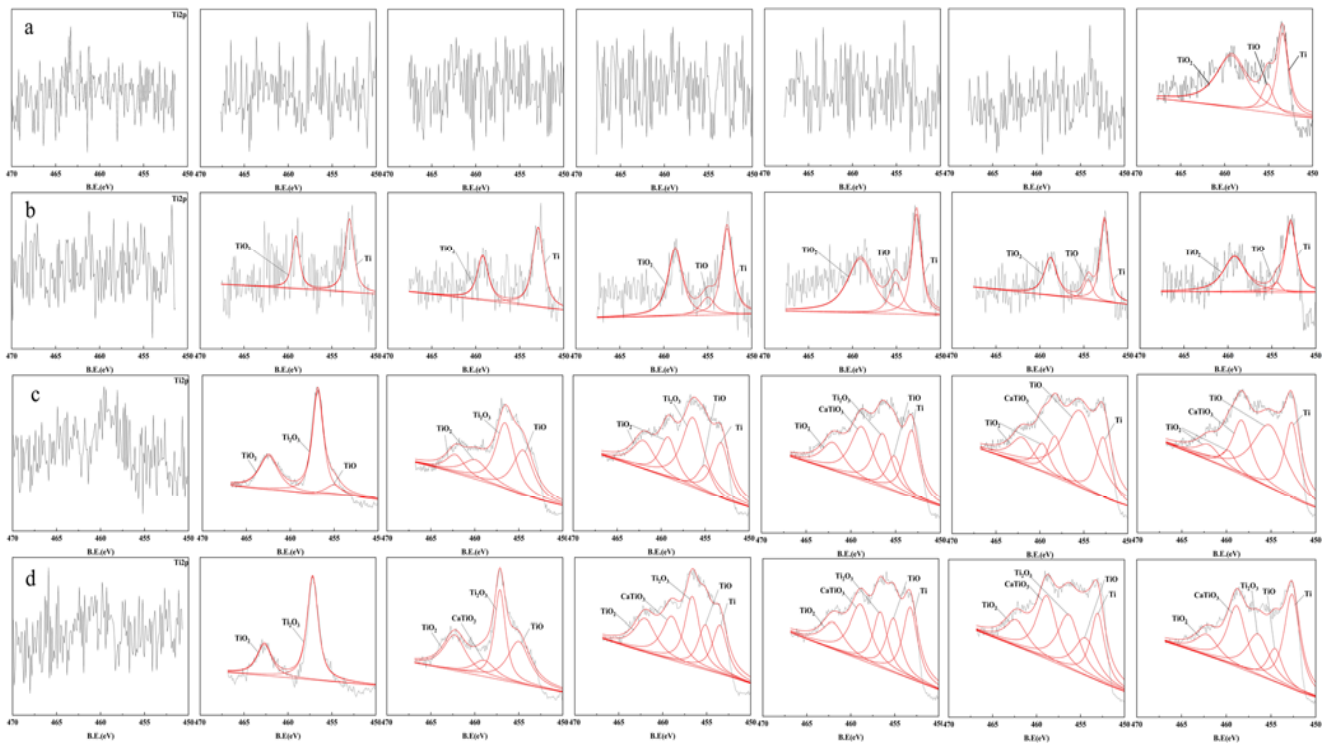


**Fig. 5.** Ti2p etching spectra of four films XPS. (a) CHA film, (b) Mg-CHA film, (c) heat-treated CHA film, (d) heat-treated Mg-CHA film.

micropores becomes clearer. The pore diameters are approximately 0.8 to 1  $\mu\text{m}$ , and the film surface exhibits extensive pore formation. In Fig. 6d, it can be seen that after soaking for 14 days, the pore-like structure completely disappears and the surface is almost completely covered by new sediment [33]. Therefore, it can be found that Mg in the heat-treated Mg-CHA film undergoes ion exchange in the SBF, and the dissolution plays a dominant role in the initial stage of immersion, forming a porous structure. In the later stage, ions reprecipitate from the solution to the surface of the film, resulting in the formation of a new apatite layer, completely covering the porous structure of the heat-treated Mg-CHA film. Compared with the Mg-HA film studied in the previous research of our research group [34], the Mg-CHA film shows significant advantages in Table 2. After 7 days of immersion, the surface of the Mg-HA film exhibits a porous structure, while the Mg-CHA film has a significantly higher pore for-

mation rate than Mg-HA. This may be attributed to the presence of more trace elements in CHA, which accelerates the pore formation rate [17, 34].

Figure 7 shows the EDX images of the Mg-CHA film soaked in SBF for 0, 3, 7, and 14 days after heat treatment. EDS images indicate that the surface of the heat-treated film contains Ca, Mg, O, C, and P elements. With the change of immersion days, significant changes are also observed in the elements on the surface of the film. The content of  $\text{Ca}^{2+}$  and  $\text{Mg}^{2+}$  gradually decreases from 0 to 7 days, indicating that  $\text{Ca}^{2+}$  and  $\text{Mg}^{2+}$  in the film migrate to SBF, forming porous structures. Therefore, doping Mg plays a crucial role in pore formation. It can be inferred that soaking a single CHA film in SBF for ion exchange is not sufficient to form porous structures. The content of  $\text{Ca}^{2+}$  increases in 7–14 days, which may be due to the formation of a new apatite layer covering the surface. This corresponds to SEM images.

**Table 2.** Comparison of pore size of Mg-CHA with related studies

	Days of immersion/sample	1 day	3 days	7 days
Pore size	CHA	-	-	-
	Mg-HA	-	-	300-500 nm
	Mg-CHA	100-200 nm	300-500 nm	0.8-1 $\mu\text{m}$

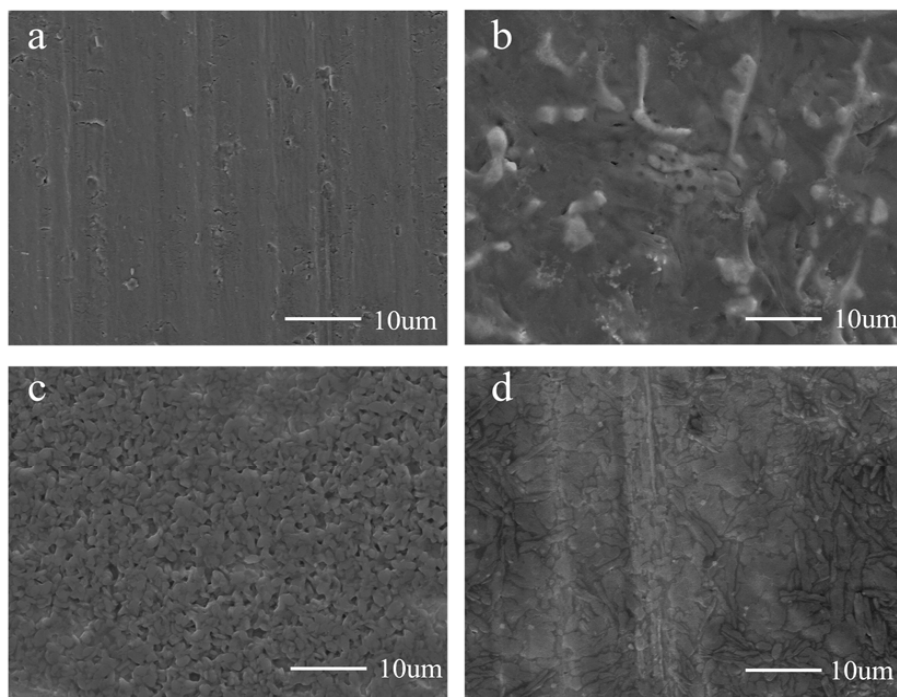


**Fig. 6.** SEM morphology of heat-treated Mg-CHA films after immersion in SBF: (a) 0 days; (b) 3 days; (c) 7 days; (d) 14 days.

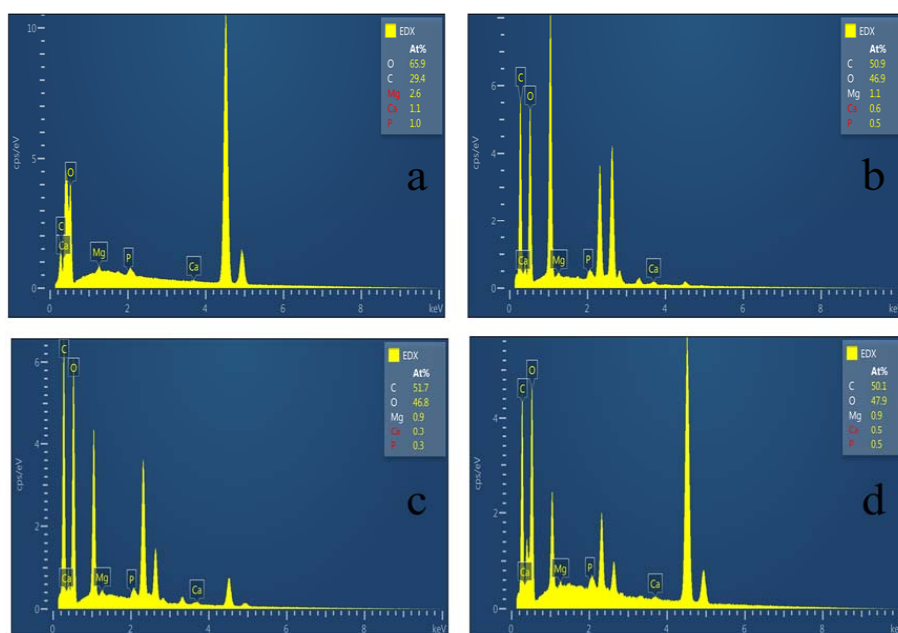


**Fig. 7.** EDX images of heat-treated Mg-CHA films immersed in SBF: (a) 0 days; (b) 3 days; (c) 7 days; (d) 14 days.

Figure 8 shows the XRD patterns of Mg-CHA films soaked in SBF at different times. From Fig. 8a, the diffraction peaks at 38.15°, 40.10°, 52.94°, and 70.48° correspond to Ti (JCDs#65-6231). After heat treatment, no crystallization peaks were observed in the Mg-CHA film except for the titanium substrate, indicating that it is an amorphous or extremely fine-grain structure [35]. From Fig. 8b, the strong diffraction peaks at 16.86° and 31.74° correspond to

HA (JCDs# 09-0432), 2θ of 22.49° and 13.79° correspond to Mg<sub>3</sub>(PO<sub>4</sub>)<sub>2</sub> (JCDs # 35-0134) and Ca<sub>3</sub>(PO<sub>4</sub>)<sub>2</sub> (JCDs # 89-4405), respectively. From Fig. 8c, a new HA diffraction peak appears at 2θ = 45.90° and the intensity of the diffraction peak at the previous position is stronger, indicating that small crystals are easier to dissolve in the physiological environment, but can also induce the formation of a new apatite layer at the early stage. By increasing the level of

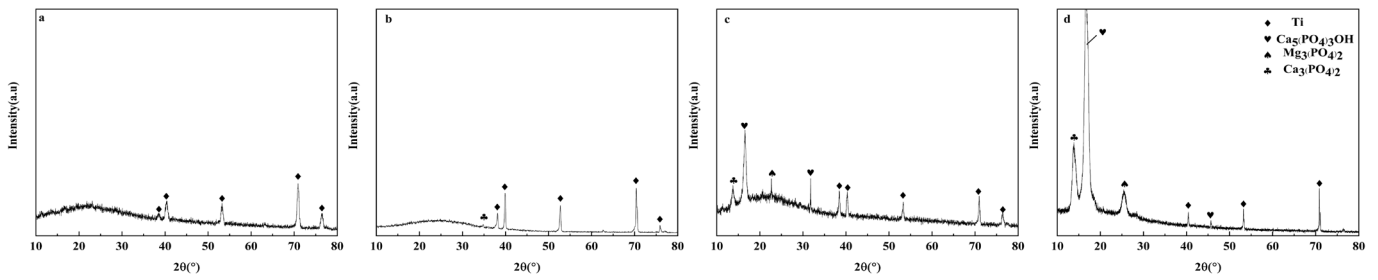


**Fig. 8.** The XRD of heat-treated Mg-CHA films immersed in SBF: (a) 0 days; (b) 3 days; (c) 7 days; (d) 14 days.

crystallinity, a stable coating should be produced. Therefore, it can be inferred that the Mg-CHA film prepared by PLD exhibits high induced activity in SBF, transforming into the HA phase. Annealing after deposition has been proven to be an effective method for converting the deposited amorphous coating into a crystalline phase [36].

Figure 9 shows the high-resolution XPS spectra of Mg2p and Ca2p before and after soaking in the heat-treated Mg-CHA film. Before immersion, the binding energy of Mg2p and Ca2p can be detected in the film. Ca2p appears in the form of CaCO<sub>3</sub> and

Ca<sub>3</sub>(PO<sub>4</sub>)<sub>5</sub>OH, and CaO appears with the deepening of etching; Among them, magnesium exists in the form of MgCO<sub>3</sub> on the surface. When etching further, it is found that magnesium exists in the form of a simple substance, and the corresponding binding energy is 49.2 eV.

Figure 10 shows that no binding energy of Mg 2p was detected after 7 days of immersion, indicating that magnesium ions in the film were released rapidly, thus forming a porous structure, which is consistent with the SEM results.

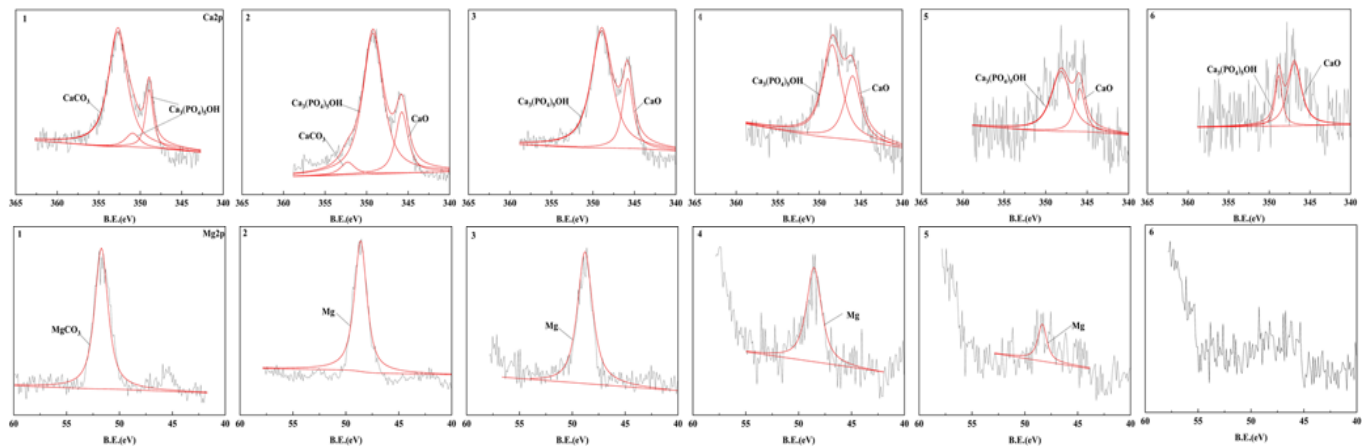


**Fig. 9.** High-resolution spectra of XPS of Mg2p and Ca2p of heat-treated Mg-CHA films before immersion.

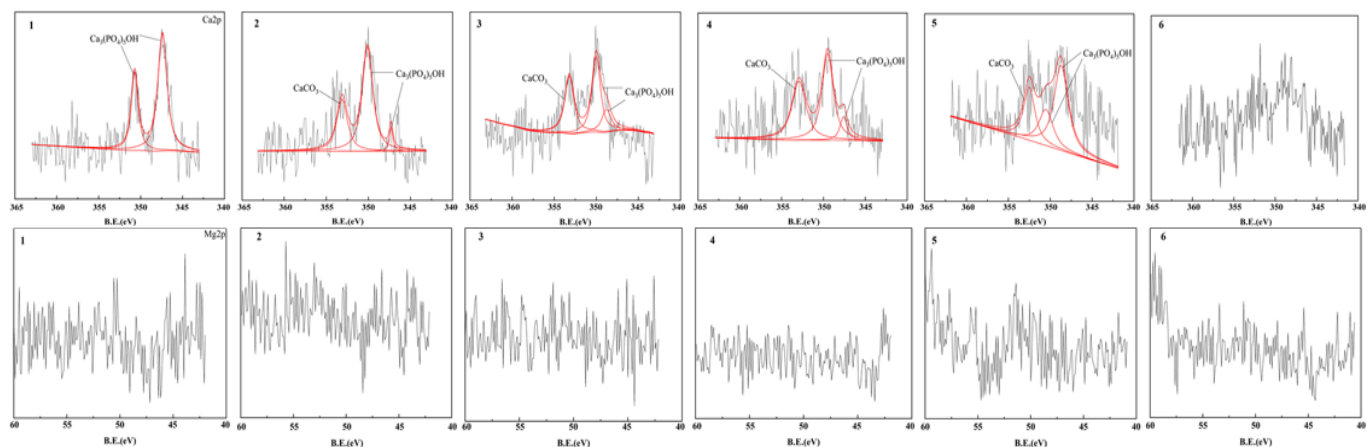


**Fig. 10.** High-resolution spectra of XPS of Mg2p and Ca2p of heat-treated Mg-CHA films immersed for 7 days.

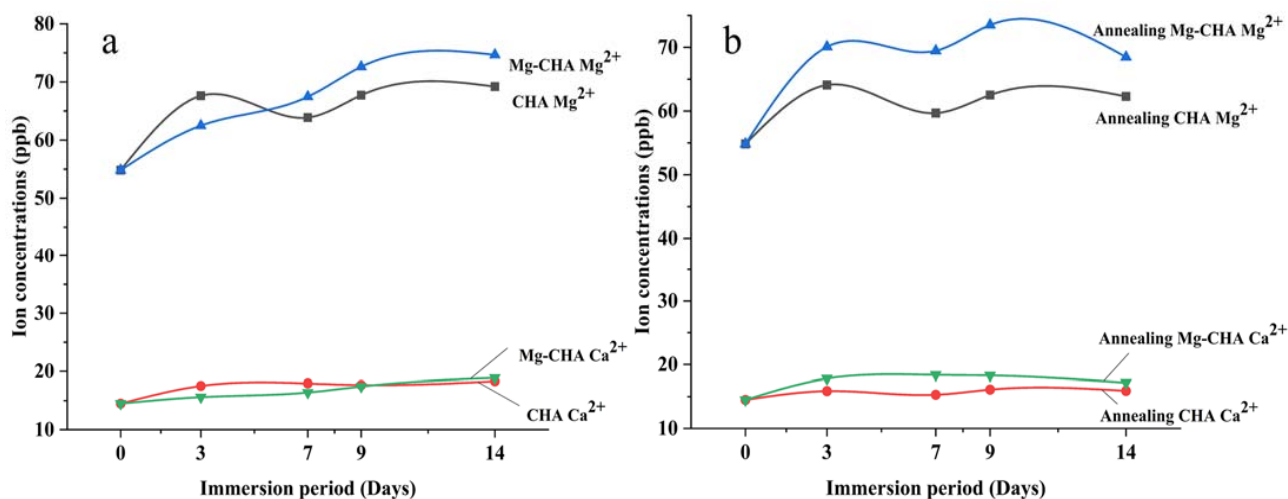


**Fig. 11.** ICP-MS plots of films immersed in SBF for 0, 3, 7, 9, and 14 days: (a) Four films before heat treatment; (b) Four films after heat treatment.

Figure 11 shows the ICP-MS image of the thin film soaked in SBF at different times. After soaking the film in SBF for different times, the change in Mg<sup>2+</sup>/Ca<sup>2+</sup> content in SBF is detected by ICP-MS to evaluate the release behavior of Mg<sup>2+</sup>/Ca<sup>2+</sup> in the film. The results are represented in [ppb], as shown in the Fig. 11. Firstly, the concentrations of Mg<sup>2+</sup> and Ca<sup>2+</sup> in the original SBF are 54.83 ppb and 14.49 ppb, respectively. As the soaking time increases, the concentrations of Mg<sup>2+</sup> and Ca<sup>2+</sup> show an upward trend, with the Mg<sup>2+</sup> concentration increasing more significantly. After heat treatment, the Mg-CHA film was soaked in SBF for 3 days, 7 days, and 14 days, with Mg<sup>2+</sup> concentrations of 70.03 ppb, 69.48 ppb, 73.58 ppb, and 68.48 ppb, respectively. Ion exchange occurs at the interface between the SBF solution and the film, where ions from the film migrate to the solution leading to dissolution of the film, and ions from the solution then precipitate onto the surface of the film leading to the formation of an apatite layer. The dissolution and reprecipitation reactions occur simultaneously, but one of the two processes dominates at different times [37]. From the graph, it can be observed that the Mg-CHA film after heat treatment is dominated by dissolution in the first seven days, and reprecipitation in the 7–14 days, which corresponds to the SEM image of mineralization.

#### 4. Conclusion

This paper analyses the effect on coating properties before and after heat treatment and draws the following conclusions:

1) The chemical composition of the deposited CHA films is consistent with the chemical composition of the original compound. Thermal treatment does not have a noticeable impact on the structure of the deposited films. Thermal treatment facilitates the oxidation of magnesium, leading to the formation of magnesium oxide (MgO). Additionally, heat treatment can promote the transformation of the amorphous structure of hydroxyapatite into a crystalline structure.

2) The effect of heat treatment is reflected in the enhanced interaction between the film and the titanium substrate, leading to increased adhesion. This increase in adhesion is attributed to the chemical interaction between the film and titanium. The role of magnesium is manifested in the increased strength of the CHA layer.

3) The presence of magnesium in the film can lead to rapid corrosion of the metal when it is immersed in a solution for an extended period. As a result of this process, a porous structure is formed. This porous structure facilitates intensive exchange reactions and the formation of a layer of hydroxyapatite. The structural rearrangement during the heat treatment process promotes the rapid corrosion of magnesium.

#### Acknowledgments

This work was supported by Intergovernmental Cooperation Projects in the National Key Research and Development Plan of the Ministry of Science and Technology of PRC (project 2022YFE0196800, for 2023-2024).

## References

- [1]. N. Xue, X. Ding, R. Huang, R. Jiang, et al., *Pharmaceuticals* 15 (2022) 879. DOI: [10.3390/ph15070879](https://doi.org/10.3390/ph15070879)
- [2]. Y. Wang, H. Zhang, Y. Hu, Y. Jing, et al., *Adv. Funct. Mater.* 32 (2022) 2208639. DOI: [10.1002/adfm.202208639](https://doi.org/10.1002/adfm.202208639)
- [3]. D. Wang, Y. Liu, Y. Liu, L. Yan, et al., *J. Biomed. Mater. Res. A* 107 (2019) 2360–2370. DOI: [10.1002/jbm.a.36744](https://doi.org/10.1002/jbm.a.36744)
- [4]. Y. Xia, H. Wang, Y. Li, C. Fu, *Front. Mater.* 9 (2022) 929618. DOI: [10.3389/fmats.2022.929618](https://doi.org/10.3389/fmats.2022.929618)
- [5]. S. Akyol, B.B. Nissan, I. Karacan, M. Yetmez, et al., *J. Aust. Ceram. Soc.* 55 (2019) 893–901. DOI: [10.1007/s41779-018-00304-4](https://doi.org/10.1007/s41779-018-00304-4)
- [6]. Ch. Daulbayev, G. Mitchell, A. Zakhidov, F. Sultanov, et al., *Eurasian Chem.-Technol. J.* 20 (2018) 119–124. DOI: [10.18321/ectj690](https://doi.org/10.18321/ectj690)
- [7]. Y. Xu, D. Wang, L. Yang, H. Tang, *Mater. Charact.* 47 (2001) 83–87. DOI: [10.1016/S1044-5803\(01\)00154-1](https://doi.org/10.1016/S1044-5803(01)00154-1)
- [8]. S.K. Nandi, B. Kundu, J. Mukherjee, A. Mahato, et al., *Mater. Sci. Eng. C* 49 (2015) 816–823. DOI: [10.1016/j.msec.2015.01.078](https://doi.org/10.1016/j.msec.2015.01.078)
- [9]. Y. Zhang, Q.-S. Yin, Y. Zhang, H. Xia, et al., *J. Mater. Sci. Mater. Med.* 21 (2010) 2453–2462. DOI: [10.1007/s10856-010-4101-x](https://doi.org/10.1007/s10856-010-4101-x)
- [10]. C. Daulbayev, F. Sultanov, A.V. Korobeinyk, M. Yeleuov, et al., *Surfaces and Interfaces* 28 (2022) 101683. DOI: [10.1016/j.surfin.2021.101683](https://doi.org/10.1016/j.surfin.2021.101683)
- [11]. H. Zhang, Y. Zhou, N. Yu, H. Ma, et al., *Acta Biomater.* 91 (2019) 82–98. DOI: [10.1016/j.actbio.2019.04.024](https://doi.org/10.1016/j.actbio.2019.04.024)
- [12]. T.E. Grenga, J.E. Zins, T.W. Bauer, The Rate of Vascularization of Coralline Hydroxyapatite, *Plastic and Reconstructive Surgery* 84 (1989) 245–249. DOI: [10.1097/00006534-198908000-00009](https://doi.org/10.1097/00006534-198908000-00009)
- [13]. S. Siswanto, D. Hikmawati, U. Kulsum, D.I. Rudyardjo, et al., *Open Chem.* 18 (2020) 584–590. DOI: [10.1515/chem-2020-0080](https://doi.org/10.1515/chem-2020-0080)
- [14]. N.C. Köseoğlu, A. Büyükkaksoy, M.H. Aslan, A.Y. Oral, *Mater. Sci. Tech.* 25 (2009) 799–804. DOI: [10.1179/174328408X353787](https://doi.org/10.1179/174328408X353787)
- [15]. W. Mróz, A. Bombalska, S. Burdyńska, M. Jedyński, et al., *J. Mol. Struct.* 977 (2010) 145–152. DOI: [10.1016/j.molstruc.2010.05.025](https://doi.org/10.1016/j.molstruc.2010.05.025)
- [16]. Y.-C. Liu, Y.-T. Lee, T.-C. Huang, G.-S. Lin, et al., *ACS Appl. Bio Mater.* 4 (2021) 2523–2533. DOI: [10.1021/acsbm.0c01535](https://doi.org/10.1021/acsbm.0c01535)
- [17]. L. Cao, I. Ullah, N. Li, S. Niu, et al., *J. Mater. Sci. Technol.* 35 (2019) 719–726. DOI: [10.1016/j.jmst.2018.10.020](https://doi.org/10.1016/j.jmst.2018.10.020)
- [18]. B. Bitá, E. Stancu, D. Stroe, M. Dumitrache, et al., *Polymers* 14 (2022) 582. DOI: [10.3390/polym14030582](https://doi.org/10.3390/polym14030582)
- [19]. N. Kanasan, S. Adzila, C.T. Koh, H.A. Rahman, G. Panerselvan, *Adv. Appl. Ceram.* 118 (2019) 381–386. DOI: [10.1080/17436753.2019.1611983](https://doi.org/10.1080/17436753.2019.1611983)
- [20]. D. Predoi, S.L. Iconaru, M.V. Predoi, M. Motelica-Heino, et al., *Coatings* 10 (2020) 510. DOI: [10.3390/coatings10060510](https://doi.org/10.3390/coatings10060510)
- [21]. F. Ren, Y. Leng, R. Xin, X. Ge, *Acta Biomater.* 6 (2010) 2787–2796. DOI: [10.1016/j.actbio.2009.12.044](https://doi.org/10.1016/j.actbio.2009.12.044)
- [22]. N.V. Bulina, O.B. Vinokurova, I.Yu. Prosanov, A.M. Vorobyev, et al., *Ceram. Int.* 48 (2022) 35217–35226. DOI: [10.1016/j.ceramint.2022.08.123](https://doi.org/10.1016/j.ceramint.2022.08.123)
- [23]. J.-Y. Wang, Y.-C. Liu, G.-S. Lin, H.-H. Chang, et al., *Surf. Coat. Tech.* 386 (2020) 125452. DOI: [10.1016/j.surfcoat.2020.125452](https://doi.org/10.1016/j.surfcoat.2020.125452)
- [24]. S. Iconaru, A. Prodan, N. Buton, D. Predoi, *Molecules* 22 (2017) 604. DOI: [10.3390/molecules22040604](https://doi.org/10.3390/molecules22040604)
- [25]. R.T. Candidato, C. Thouzellier, L. Pawłowski, *J. Biomed. Mater. Res.* 106 (2018) 2101–2108. DOI: [10.1002/jbm.b.34014](https://doi.org/10.1002/jbm.b.34014)
- [26]. S. Singh, K.K. Pandey, A.K. Keshri, *Met. Mater. Int.* 27 (2021) 4455–4462. DOI: [10.1007/s12540-020-00704-x](https://doi.org/10.1007/s12540-020-00704-x)
- [27]. M. Ohki, S. Takahashi, R. Jinnai, T. Hoshina, *J. Therm. Spray Tech.* 29 (2020) 1119–1133. DOI: [10.1007/s11666-020-01041-6](https://doi.org/10.1007/s11666-020-01041-6)
- [28]. U.R. Eckstein, R. Detsch, N.H. Khansur, M. Brehl, et al., *Ceram. Int.* 45 (2019) 14728–14732. DOI: [10.1016/j.ceramint.2019.04.197](https://doi.org/10.1016/j.ceramint.2019.04.197)
- [29]. M. Maximov, O.-C. Maximov, L. Craciun, D. Ficai, et al., *Coatings* 11 (2021) 1386. DOI: [10.3390/coatings11111386](https://doi.org/10.3390/coatings11111386)
- [30]. Q. Bao, C. Chen, D. Wang, J. Liu, *Cryst. Growth Des.* 8 (2008) 219–223. DOI: [10.1021/cg070151e](https://doi.org/10.1021/cg070151e)
- [31]. A. Rezaei, R.B. Golenji, F. Alipour, M.M. Hadavi, et al., *Ceram. Int.* 46 (2020) 25374–25381. DOI: [10.1016/j.ceramint.2020.07.005](https://doi.org/10.1016/j.ceramint.2020.07.005)
- [32]. Y. Su, D. Li, Y. Su, C. Lu, et al., *ACS Biomater. Sci. Eng.* 2 (2016) 818–828. DOI: [10.1021/acsbomaterials.6b00013](https://doi.org/10.1021/acsbomaterials.6b00013)
- [33]. Z. Chen, J. Zhai, D. Wang, C. Chen, *Ceram. Int.* 44 (2018) 10204–10209. DOI: [10.1016/j.ceramint.2018.03.013](https://doi.org/10.1016/j.ceramint.2018.03.013)
- [34]. J. Cao, X. Liu, X. Jiang, R. Lian, et al., *Appl. Surf. Sci.* 565 (2021) 150598. DOI: [10.1016/j.apsusc.2021.150598](https://doi.org/10.1016/j.apsusc.2021.150598)
- [35]. S. Johnson, M. Haluska, R.J. Narayan, R.L. Snyder, *Mater. Sci. Eng. C* 26 (2006) 1312–1316. DOI: [10.1016/j.msec.2005.08.023](https://doi.org/10.1016/j.msec.2005.08.023)
- [36]. N. Ohtsu, S. Hiromoto, M. Yamane, K. Satoh, et al., *Surf. Coat. Tech.* 218 (2013) 114–118. DOI: [10.1016/j.surfcoat.2012.12.037](https://doi.org/10.1016/j.surfcoat.2012.12.037)
- [37]. J. Weng, *Biomaterials* 18 (1997) 1027–1035. DOI: [10.1016/S0142-9612\(97\)00022-7](https://doi.org/10.1016/S0142-9612(97)00022-7)